Check for updates

A Journal of the Gesellschaft Deutscher Chemiker

Angewandte International Edition Chemie

GDCh

www.angewandte.org

Accepted Article

Title: Designing Solvated Double-Layer Polymer Electrolytes with Molecular Interactions Mediated Stable Interfaces for Sodium Ion Batteries

Authors: Jun Pan, Yuchen Zhang, Fu Sun, Markus Osenberg, André Hilger, Ingo Manke, Ruiguo Cao, Shixue Dou, and Hongjin Fan

This manuscript has been accepted after peer review and appears as an Accepted Article online prior to editing, proofing, and formal publication of the final Version of Record (VoR). The VoR will be published online in Early View as soon as possible and may be different to this Accepted Article as a result of editing. Readers should obtain the VoR from the journal website shown below when it is published to ensure accuracy of information. The authors are responsible for the content of this Accepted Article.

To be cited as: *Angew. Chem. Int. Ed.* **2023**, e202219000

Link to VoR: https://doi.org/10.1002/anie.202219000

WILEY VCH

15213773, ja, Downloaded from https://onlinelibrary.wiley.com/doi/10.1002/anie.202219000 by NANYANG TECHNOLOGICAL UNIVERSITY, Wiley Online Library on [04/03/2023]. See the Terms and Conditions (https://onlinelibrary.wiley.com/terms-and-conditions) on Wiley Online Library for rules of use; OA articles are governed by the applicable Creative Commons License

10.1002/anie.202219000

WILEY-VCH

Designing Solvated Double-Layer Polymer Electrolytes with Molecular Interactions Mediated Stable Interfaces for Sodium Ion Batteries

Jun Pan,[a]# Yuchen Zhang,[b]# Fu Sun,[c] Markus Osenberg,[d] André Hilger,[d] Ingo Manke,[d] Ruiguo Cao,[b] Shi Xue Dou,[e] Hong Jin Fan[a]*

Abstract: *Unstable cathode-electrolyte and/or anode-electrolyte interface in polymer-based sodium-ion batteries (SIBs) will deteriorate their cycle performance. Herein, a unique solvated double-layer quasi-solid polymer electrolyte (SDL-QSPE) with high Na^+ ion conductivity is designed to simultaneously improve stability on both cathode and anode sides. Different functional fillers are solvated with plasticizers to improve Na^+ conductivity and thermal stability. The SDL-QSPE is laminated by cathode- and anode-facing polymer electrolyte to meet the independent interfacial requirements of the two electrodes. The interfacial evolution is elucidated by theoretical calculations and* 3D X-ray microtomography analysis*. The $Na_{0.67}Mn_{2/3}Ni_{1/3}O_2$|SDL-QSPE|Na batteries exhibit 80.4 mAh g^{-1} after 400 cycles at 1 C with the Coulombic efficiency close to 100%, which significantly outperforms those batteries using the monolayer-structured QSPE.*

Sodium-ion batteries (SIBs) are promising for large-scale energy storage due to their low cost and compatibility with the current lithium-ion battery production technology.[1] Nevertheless, similar to Li-ion batteries that use flammable liquid electrolyte, there exist safety concerns for liquid electrolytes based SIBs.[2,3] Although the flexible solid polymer electrolyte is acknowledged as a good strategy to solve this problem, its low ionic conductivity limits its wide adoption.[4-8] The quasi-solid polymer electrolytes (QSPEs), which combine the advantages of liquid electrolytes and polymer electrolytes to achieve good ionic conductivity and enhanced electrochemical stability, emerge as a more promising solution.[9,10]

Previous studies demonstrate that the interfacial stability between QSPE and electrode govern largely the overall performance of the SIBs.[11] The interfacial instability at the cathode is mainly caused by the decomposition of the electrolyte, the process of which can be catalysed by the released cathode transition metal ions and further exacerbated by the acid by-products.[12] At the anode, the reductive Na metal may lead to the decomposition of the electrolyte during Na stripping, and the repeated expansion/contraction of Na metal during cycling will deteriorate the physical contact at the anode/electrolyte interface.[13] These detrimental effects have set grand challenge for implementing QSPE in commercial batteries. As a result, it is necessary to design and build a protective dense cathode-electrolyte interphase (CEI) film and a buffered high reduction-resistant anode/electrolyte interface. It is demonstrated that a single targeted CEI or solid-electrolyte interphase can be obtained by deliberately tailoring the electrolyte compositions (either polymer, sodium salt, filler, or plasticizer).[14] However, simultaneously constructing stable interfaces to meet the different requirements of both cathode and anode has been rarely reported. Therefore, new designing strategies for QSPEs are needed to simultaneously construct stable cathode-electrolyte and anode-electrolyte interfaces while maintaining high ionic conductivity.

To achieve the goal, herein, a solvated double-layer quasi-solid polymer electrolyte (SDL-QSPE) with high Na^+ ion conductivity is designed. This solvated double layered structure is formed via laminating a cathode-facing QSPE layer (C-QSPE) and an anode-facing QSPE layer (M-QSPE). The former contains sodium bis(trifluoromethylsulfonyl)imide (NaTFSI), poly(vinylidene fluoride-co-hexafluoropropylene) (PVDF-HFP), propylene carbonate (PC), and cellulose acetate (CA). The latter M-QSPE contains NaTFSI, PVDF-HFP, PC, and molecular sieve (MS). The two different functional fillers (CA and MS) are chosen to meet the independent interfacial requirements of both cathode and anode and they are both solvated with PC plasticizer to increase the Na^+ ion conductivity and the thermal stability of the prepared QSPE. With this subtle design, the unwanted interfacial side reactions at both the cathode and anode in SIBs are significantly suppressed due to the formation of robust interfaces, as demonstrated by the density functional theory (DFT), Fourier transform infrared (FTIR), X-ray photoelectron spectroscopy (XPS), electron microscopy, and synchrotron X-ray tomography characterizations. The fabricated $Na_{0.67}Mn_{2/3}Ni_{1/3}O_2$ (NMNO)|SDL-QSPE|Na batteries exhibit significantly improved cycle life than those batteries using a single-layer structure electrolyte (either C-QSPE or M-QSPE). These results demonstrate that the solvated double-layer design is beneficial for the development of polymer-based SIBs towards long cycle life and high safety.

Figure 1a schematically displays the SIB structure using the proposed solvated double-layer quasi-solid polymer electrolyte (SDL-QSPE). The SDL-QSPE is a laminate of a CA-filled QSPE close to the cathode side (C-QSPE) and a MS-filled QSPE at the anode side (M-QSPE), both of which employ PC plasticizer. Organic CA and inorganic MS are selected respectively as the cathode and anode fillers due to their high liquid absorption capability and various functional groups. In the current design, a solvated structure between the functional fillers (CA and MS)

[a] School of Physical and Mathematical Sciences, Nanyang Technological University, Singapore 637371, Singapore. *E-mail: fanhj@ntu.edu.sg
[b] Hefei National Laboratory for Physical Science at the Microscale, CAS Key Laboratory of Materials for Energy Conversion, Department of Materials Science and Engineering, University of Science and Technology of China, Hefei 230026, China.
[c] Qingdao Institute of Bioenergy and Bioprocess Technology, Chinese Academy of Sciences, Qingdao 266101, China.
[d] Helmholtz-Zentrum Berlin für Materialien und Energie, Hahn-Meitner-Platz 1, Berlin 14109, Germany.
[e] Institute of Energy Materials Science, University of Shanghai for Science and Technology, Shanghai 200093, China.

This article is protected by copyright. All rights reserved.

15213773, ja, Downloaded from https://onlinelibrary.wiley.com/doi/10.1002/anie.202219000 by NANYANG TECHNOLOGICAL UNIVERSITY, Wiley Online Library on [04/03/2023]. See the Terms and Conditions (https://onlinelibrary.wiley.com/terms-and-conditions) on Wiley Online Library for rules of use; OA articles are governed by the applicable Creative Commons License

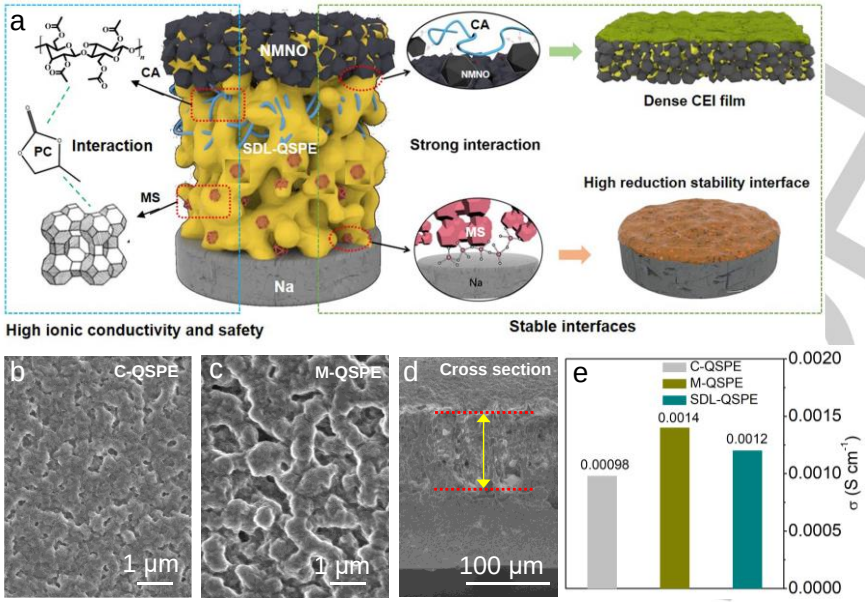

Figure 1. Design principle and characterization results of the proposed SDL-QSPE. a) Schematic illustration for the design principle of SDL-QSPE (left) and the electrode-electrolyte interfaces (right). SEM images of the cathode-facing side b), the anode-facing side c), and the cross-section of the prepared SDL-QSPE d). e) The ionic conductivity of the prepared LSD-QSPE together with the C-QSPE and M-QSPE control samples.

and the PC plasticizer will be formed due to their intermolecular force. In this way, the high ionic conductivity of the C-QSPE and M-QSPE precursors can be obtained, which is a prerequisite for preparing the high Na^+ ion conductive SDL-QSPE (see below). In addition, the solvated state between the fillers and PC will enhance the thermal stability of the SDL-QSPE and the safety property of the built SIB will not be compromised by the presence of the bonding liquid. Meanwhile, different functional fillers (CA and MS) are incorporated in C-QSPE and M-QSPE precursors to solve the different interfacial challenges of the cathode and anode in SIBs for the following reasons. At the cathode side, CA not only interacts with oxygen atoms in the cathode to help form a dense CEI film, but also acts as sticky molecules to increase the interfacial contact between the NMNO and the C-QSPE (Figure 1a, top figures in the cyan dash rectangle). At the anode side, a highly reduction-resistant anode interface is constructed between the basic sites of the MS filler and metallic Na, with the derived NaF-rich buffer interfacial layer protecting the Na anode (Figure 1a, bottom figures in the cyan dash rectangle). It is expected that this unique SDL-QSPE structure could simultaneously meet the interfacial requirements of both cathode and anode in SIBs while possessing high Na^+ ionic conductivity.

The detailed morphology, structure, and Na^+ ion conductivity properties of the prepared SDL-QSPE are characterized. The C-QSPE and M-QSPE exhibit distinctively contrasting morphologies (Figure 1b and c): a homogeneous and dense C-QSPE which facilitates uniform and intimate interfacial contact, versus a heterogeneous and three-dimensional (3D) M-QSPE which provides multiple channels for the transport of sodium ions.[15a] The cross-sectional view (Figure 1d) reveals that the laminated SDL-QSPE does not show an obvious contrast between the double layers, mainly due to their similar ingredients (NaTFSI, PVDF-HFP, and PC). The good compatibility between the M-QSPE and the C-QSPE is favorable as it maintains the mechanical strength of the whole laminated electrolyte, which would alleviate the growth of sodium dendrites.[15b] Additionally, this interfacial compatibility also helps to maintain a low interfacial resistance.[15c] The Na^+ ion conductivity of SDL-QSPE is about 1.2×10^{-3} S cm^{-1}, which sits between C-QSPE (0.98×10^{-3} S cm^{-1}) and M-QSPE (1.4×10^{-3} S cm^{-1}) (Figure 1e and S1). The higher Na^+ ion conductivity of M-QSPE than C-QSPE can be explained by a stronger binding ability of MS to the solvent,[15d] which is confirmed by the thermogravimetric analysis (TGA) (Figure S2). The decomposition voltage of SDL-QSPE is about 5 V according to the linear sweep voltage (LSV) characterization (Figure S3), which suggests that the PC solvent is firmly bonded with fillers.

The high Na^+ ion conductivity of the prepared SDL-QSPE is attributed to its reduced polymer crystallinity by incorporating the amorphous CA and MS fillers, as shown by their X-ray diffraction (XRD) patterns (Figure S4).[16a] In addition, both the CA and MS fillers are nano-sized round-shaped particles (Figure S5). This feature is also beneficial to high Na^+ ion conduction, as they can not only disperse uniformly in the electrolyte solution but also expose active sites for binding with the PC solvent. The detailed scanning electron microscope (SEM), transmission electron microscope (TEM), high-resolution TEM (HRTEM), XRD, and specific surface area characterization results of the employed NMNO cathode material are shown in the Supporting Information (Figure S6-10).

The solvated electrolyte structures formed between the functional-group-containing fillers (CA and MS) and PC were fundamentally studied by DFT calculation. Figure 2a shows the calculated electrostatic potential of the solvent and fillers. The interactions between the filler (CA/MS) and PC are manifested

This article is protected by copyright. All rights reserved.

15213773, ja, Downloaded from https://onlinelibrary.wiley.com/doi/10.1002/anie.202219000 by NANYANG TECHNOLOGICAL UNIVERSITY, Wiley Online Library on [04/03/2023]. See the Terms and Conditions (https://onlinelibrary.wiley.com/terms-and-conditions) on Wiley Online Library for rules of use; OA articles are governed by the applicable Creative Commons License

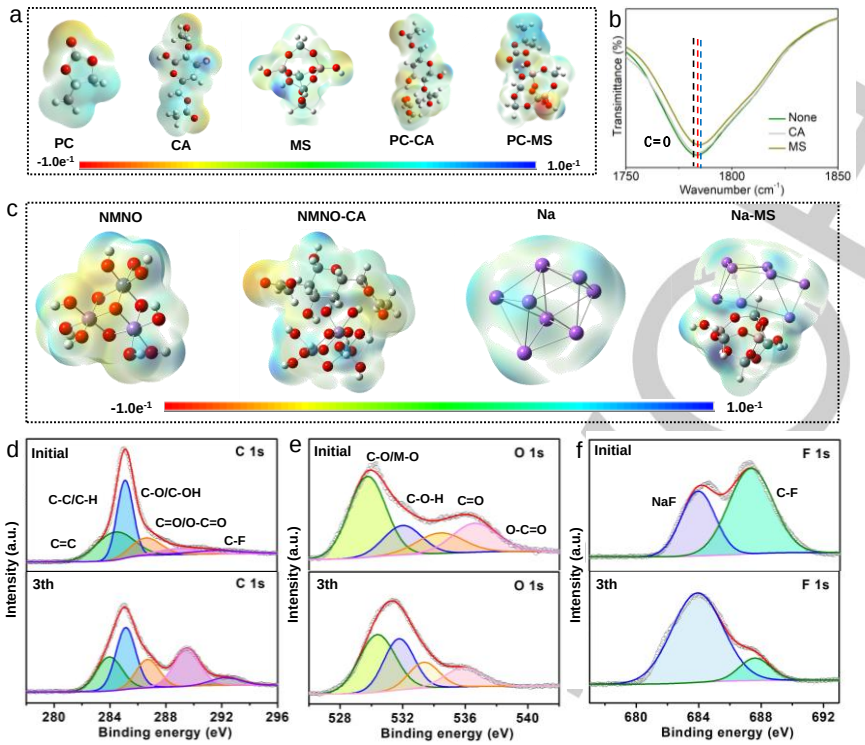

Figure 2. Density functional theory (DFT), Fourier transform infrared (FTIR) and X-ray photoelectron spectroscopy (XPS) results of the electrode-QSPE interface. a) The electrostatic potential distributions of solvents and fillers. b) FTIR spectra of C-QSPE, M-QSPE and filler-free QSPE. c) Electrostatic potential of NMNO, NMNO-CA, Na, and Na-MS. d-f) XPS characterization of the C 1s, O 1s, and F 1s at the cathode side before and after 3-cycles battery cycling.

by 1) the adsorption energy between the acidic hydroxyl groups of CA and the basic carbonyl sites in PC is -25.69 kJ/mol, and 2) the adsorption energy between the acidic Al-O-Si sites of MS and PC is -28.65 kJ/mol (Table S1). These results suggest that the PC solvent can be well complexed by CA and MS to form a solvation structure, which may restrain the flowability of the solvent and enhance the Na^+ ion conductivity.[16b] To further confirm the interactions between the filler (CA/MS) and PC, Fourier transform infrared (FTIR) spectra of C-QSPE, M-QSPE and filler-free QSPE are compared (Figure 2b). A blue shift in the filler-contained QSPE compared with the filler-free sample is observed, indicating bonding interaction between the filler and PC.[16c] This blue shift of C=O is due to the difference in the permittivity of ambient interface, which is consistent with the calculated infrared spectra (Figure S11).

The underlying interactions between the electrodes and fillers are further analyzed in DFT calculation. Figure 2c displays the DFT calculation results of the electrostatic potential of the optimized structures of NMNO, NMNO-CA, Na, and Na-MS (Figure S12 and Table S1).[17a] At the cathode, the oxygen of NMNO interacts heavily with the carbonyl groups in PC, and the adsorption energy is calculated to be -113.5 kJ/mol (Table S2). Molecular orbital theory is useful for further analyzing the potential redox reactions at the NMNO/CA interface (Figure S13).[17b] The highest occupied molecular orbital (HOMO) is close to Ni, indicating that Ni can be easily oxidized. The lowest unoccupied molecular orbital (LUMO) is in the position of Mn so that Mn can be easily reduced (Figure S13a). Accordingly, NMNO undergoes reduction and CA experiences oxidation at the interface (Figure S13b). This redox-derived by-product will generate a CEI film that covers NMNO (see below the XPS results).[17c] At the anode side, it is found that the oxygen-basic sites of the Si-O-Si groups from MS interact strongly with the Na anode, and their adsorption energy is calculated to be -510.5 kJ/mol (Table S2). For Na clusters, the electrons are delocalized and uniformly distributed, which are consistent with the simulated metallic properties (Figure S13c). The LUMO energy of the Na metal becomes higher when it is in contact with MS, indicating an improved reduction resistance (Figure S13d and Table S3).[17d]

XPS spectroscopy was conducted to analyze the interfacial bonding and compositions of the formed film before and after battery cycling. The C 1s results and the detected peaks at 284.5, 285.1, 286.7, 289.1, and 292.4 eV can be attributed to C=C, C-C/C-H, C-O/C-OH, C=O/O-C=O, and C-F, respectively (Figure 2d).[18a] The ratio of C=O/O-C=O increases after the battery is cycled, which is caused by the participation of PC in the CEI film, as evidenced by our previous work.[15c] In addition, the O 1s peaks at 529.7, 532.0, 534.5 and 536.6 eV belong to C-O/M-O, C-OH, C=O and O-C=O, respectively (Figure 2e).[18b] On the basis of the evolved content ratio of M-O and C-OH, one can note a clear decrease of M-O after cycling, indicating that the cathode is coated by a dense CEI film, which is confirmed by the TEM results (Figure S14). In addition to the organic components, it is also found that the cycled CEI becomes rich in NaF after cycling (Figure 2f). On the anode side, a NaF-rich

This article is protected by copyright. All rights reserved.

15213773, ja, Downloaded from https://onlinelibrary.wiley.com/doi/10.1002/anie.202219000 by NANYANG TECHNOLOGICAL UNIVERSITY, Wiley Online Library on [04/03/2023]. See the Terms and Conditions (https://onlinelibrary.wiley.com/terms-and-conditions) on Wiley Online Library for rules of use; OA articles are governed by the applicable Creative Commons License

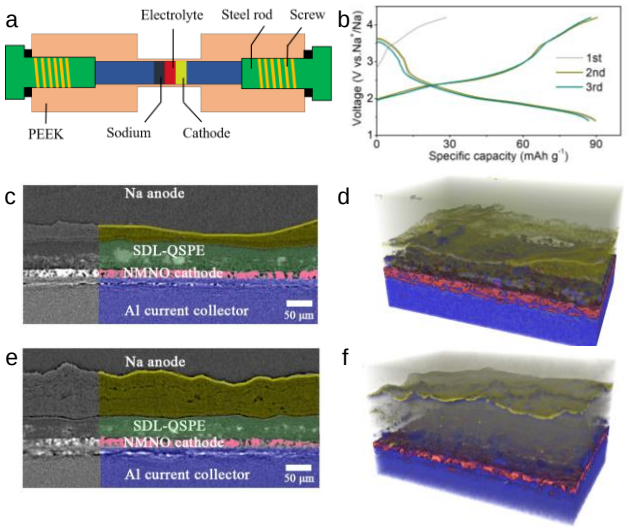

Figure 3. *Ex-situ* 3D X-ray microtomography analysis. a) Schematic diagram of the used battery design for SX-CT measurement. b) Selected charge/discharge curves of the studied cell. Selected cross-section views of the SIB after 10 cycles (c) and after 100 cycles (e). d, f) The corresponding 3D volume rendering of the tomography results in c, e. The electrochemical cycling data of these two cells are shown in Figure S16.

interface is also confirmed by XPS (Figure S15). The formed organic-inorganic hybrid interfacial film at the cathode is expected to prevent the release of transition metal ions to decompose the QSPE.[18c] Additionally, the NaF-rich buffer layer at the anode will effectively protect the Na anode and prevent Na dendrites from damaging the QSPE.[18d]

Non-destructive and three-dimensional synchrotron X-ray computed tomography (SX-CT) was used to further reveal the interface evolution of SIBs after cycling (Figure 3).[19a] The cells used for SX-CT characterization showed an unobvious voltage plateau compared to the coin cells, which could be due to the difference in current density and the effect of SX-CT cell conductivity (Figure 3b). Nevertheless, the customized SX-CT cell design is useful for studying the electrochemical reactions consistently. Two cycled SIBs (10 cycles and 100 cycles, the electrochemical curves are shown in Figure S17) were measured using SX-CT without cell disassembly (Figure 3c-f). The distinguishable structures representing different cell components are resulted from their different degrees of X-ray absorption.[19b] Figure 3c and d show that, compared with the flat and smooth Na/SDL-QSPE interface in the uncycled cell (Figure S16), a porous and heterogeneous interphase layer between Na anode and SDL-QSPE is generated after battery cycling (yellow shadow). For the 100-cycled cell, the porous and heterogeneous interphase layer becomes thicker and more porous (Figure 3e and f). This finding of a porous interphase layer at the anode side in cycled SIBs is consistent to previous reports.[19c,19d] Based on the fact that the thickness of this porous interphase layer gradually increases as a function of cycle numbers, it is reasonably to infer that this porous interphase layer is mostly electrochemically inactive. Despite of this interphase layer, one can note from Figure 3c-f that the SDL-QSPE/Interphase interface maintains its intimate contact during cycling, as the LSD-QSPE/NMNO interface does. The maintained physical contact between cathode and SDL-QSPE may result from the CA filler that functions as a powerful glue; The stable interface between the SDL-QSPE and the generated interphase may be caused by the derived NaF buffer layer that is thermodynamically stable (see the above DFT and XPS results). These results suggest that the proposed SDL-QSPE benefits long-term cyclability of the battery.

The electrochemical performance of the NMNO|SDL-QSPE|Na SIBs was extensively studied (Figure 4). The specific capacity of NMNO|SDL-QSPE|Na battery after 400 cycles at 1 C is 80.4 mAh g^{-1} and the corresponding Coulombic efficiency is close to 100% (Figure 4a and S18a), which is superior to those SIBs using the control samples (C-QSPE and M-QSPE). In the selected charge-discharge curves (Figure 4b), the redox platforms around 3.0 V are attributed to the $Ni^{2+}/Ni^{3+}/Ni^{4+}$ redox reaction, while the platforms located around 2 V are due to Mn^{3+}/Mn^{4+} redox reaction.[20a] The NMNO|SDL-QSPE|Na SIBs also possess superior rate capability (Figure 4c); Specifically, the available capacities of 149.1, 138.8, 125.8, 105.7, and 64.6 mAh g^{-1} are obtained at 0.2, 0.5, 1, 2, and 5 C, respectively, which are higher than the SIBs using either the C-QSPE or M-QSPE control samples and outperforms most of the reported gel electrolyte-based layered cathode (Figure S18b and Table S4). When the current rate is restored to 0.2 C, the available capacity is 145.6 mAh g^{-1}. Electrochemical impedance spectroscopy (EIS) and galvanostatic intermittent titration technique (GITT) were employed to reveal the inner resistance evolution of the NMNO|SDL-QSPE|Na SIBs (Figure 4d and S19, and Table S5). The charge transfer resistance (R_{ct}) and the interface resistance (R_f) of NMNO|SDL-QSPE|Na SIB after 5 cycles are smaller than those of the SIBs using the control samples. Smaller resistance indicates fast reaction kinetics and a stable interface after activation, which is favorable for rate performance.[20b] In addition, the GITT results (Figure S20) suggest that the internal resistance is about 900 Ω during the charging process, and it increases continuously during the discharging. The continuously

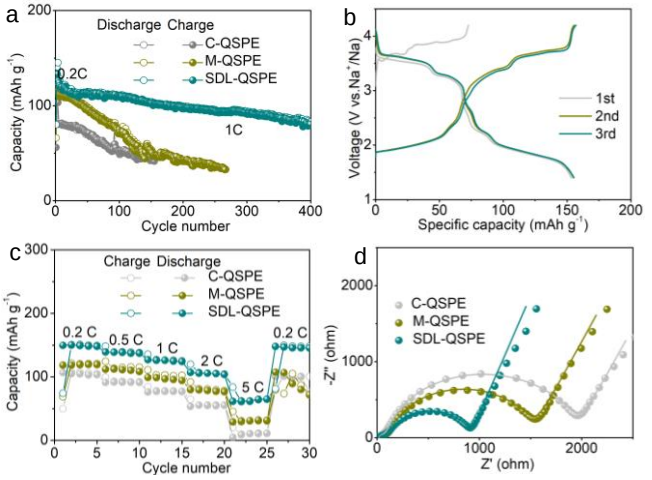

Figure 4. Electrochemical properties of the fabricated SIBs. a) Cycling performances of the SIBs built using different electrolytes at current density of 1 C, where 1 C=100 mAh g^{-1}. b) Selected charge/discharge curves of the NMNO|SDL-QSPE|Na for the first three cycles. c) Rate performances test of the SIBs built using different electrolytes. d) EIS spectra of the SIBs built using different electrolytes after 5 cycles.

This article is protected by copyright. All rights reserved.

15213773, ja, Downloaded from https://onlinelibrary.wiley.com/doi/10.1002/anie.202219000 by NANYANG TECHNOLOGICAL UNIVERSITY, Wiley Online Library on [04/03/2023]. See the Terms and Conditions (https://onlinelibrary.wiley.com/terms-and-conditions) on Wiley Online Library for rules of use; OA articles are governed by the applicable Creative Commons License

Accepted Manuscript

increased inner resistance is very likely caused by the formed porous interphase layer between Na and SDL-QSPE (see the above SX-CT results), which is disadvantageous for fast Na^+ ions transportation.[20c]

In summary, we have designed a unique quasi-solid polymer electrolyte with high Na^+ ion conductivity to simultaneously fulfill the requirements of cathode and anode in Na-ion batteries. This is achieved by choosing different functional fillers (superabsorbent organic CA and inorganic MS) in constructing the quasi-solid-state electrolyte. First, the intermolecular force between the hydroxyl groups of CA or the acidic sites of MS and the C=O groups of PC forms a solvated structure. The solvated structure between the fillers and the PC plasticizer not only guarantees high ionic conductivity of the polymer electrolyte but also helps to improve the safety property of the SIB by restraining the free mobile PC. Furthermore, the double-layer structure of this polymer electrolyte, which is formed by laminating the CA-filled QSPE at the cathode side and the MS-filled QSPE at the anode side, contributes to the formation of stable cathode-electrolyte and anode-electrolyte interfaces via strongly molecular interactions between the electrode and corresponding filler (CA-NMNO and MS-Na). The stable interfaces are verified by XPS and ex-situ 3D X-ray microtomography characterizations. With this electrolyte design, the fabricated NMNO|SDL-QSPE|Na battery exhibits a capacity of 80.4 mAh g^{-1} after 400 cycles at 1 C, which is significantly higher than those batteries using monolayer-structure electrolytes (viz., C-QSPE and M-QSPE). This strategy of simultaneously enhancing the Na^+ ion conductivity and the interfacial stability at the electrodes through a unique solvation and double-layer structure is promising for achieving high-performance sodium ion batteries.

Acknowledgements

This work was financially supported by the National Nature Science Foundation of China (No. 22209199, 52101276). H. J. F. acknowledges the financial support from Ministry of Education, Singapore, by its Academic Research Fund Tier 1 (RG85/20) and Tier 2 (MOE-T2EP50121-0006). The authors acknowledge Helmholtz-Zentrum Hereon (Geesthacht, Germany) for provision of the PETRA III P05 beamline and conducting the synchrotron X-ray tomography measurements as well as DESY (Hamburg, Germany) for operating the PETRA III synchrotron facility. The authors thank Dr. Fabian Wilde for aiding in conducting the synchrotron X-ray tomography measurements.

Keywords: Functional filler • Double-layer polymer electrolytes • Stable interfaces • Molecular intercalation • Quasi-solid-state sodium ion batteries

[1] a) J. Y. Hwang, S. T. Myung, Y. K. Sun, *Chem. Soc. Rev.* **2017**, *46*, 3529-3614; b) A. Kumar, Nagmani, S. Puravankara, *Mater. Today Energy* **2022**, *29*, 101115; c) D. Kundu, E. Talaie, V. Duffort, L. F. Nazar, *Angew. Chem. Int. Ed.* **2015**, *54*, 3431-3448.

[2] a) P. K. Nayak, L. T. Yang, W. Brehm, P. Adelhelm, *Angew. Chem. Int. Ed.* **2018**, *57*, 102-120; b) C. Li, F. Geng, B. Hu, B. Hu, *Mater. Today Energy* **2020**, *17*, 100474.

[3] a) Z. N. Tian, Y. G. Zou, Y. Z. Wang, J. Yin, J. Ming, H. N. Alshareef, *Adv. Sci.* **2022**, *9*, 2201207; b) Y. Y. Hu, R. X. Han, L. Mei, J. L. Liu, J. C. Sun, K. Yang, J. W. Zhao, *Mater. Today Energy* **2021**, *19*, 100608.

[4] a) F. Gebert, J. Knott, R. Gorkin III, S. L. Chou, S. X. Dou, *Energy Storage Mater.* **2021**, *36*, 10-30; b) G. Y. Du, M. L. Tao, J. Li, T. T. Yang, W. Gao, J. H. Deng, Y. R. Qi, S. J. Bao, M. W. Xu, *Adv. Energy Mater.* **2020**, *10*, 1903351; c) C. Sangeland, R. Younesi, J. Mindemark, D. Brandell, *Energy Storage Mater.* **2019**, *19*, 31-38.

[5] H. C. Gao, S. Xin, L. G. Xue, J. B. Goodenough, *Chem* **2018**, *4*, 833-844.

[6] a) Y. Yao, Z. Y. Wei, H. Y. Wang, H. J. Huang, Y. Jiang, X. J. Wu, X. Y. Yao, Z. S. Wu, Y. Yu, *Adv. Energy Mater.* **2020**, *10,* 1903698; b) Q. Yi, W. Q. Zhang, S. Q. Li, X. Y. Li, C. W. Sun, *ACS Appl. Mater. Interfaces* **2018**, *10*, 35039-35046.

[7] a) X. X. Wang, Z. H. Liu, Y. H. Tang, J. J. Chen, Z. Y. Mao, D. J. Wang, *Solid State Ionics* **2021**, *359*, 115532; b) J. F. Wu, Z. Y. Yu, Q. Wang, X. Guo, *Energy Storage Mater.* **2020**, *24*, 467-471.

[8] a) C. T. Zhou, S. Bag, V. Thangadurai, *ACS Energy Lett.* **2018**, *3*, 2181-2198; b) C. L. Zhao, L. L. Liu, X. G. Qi, Y. X. Lu, F. X. Wu, J. M. Zhao, Y. Yu, Y. S. Hu, L. Q. Chen, *Adv. Energy Mater.* **2018**, *8*, 1703012.

[9] a) C. D. Zhao, J. Z. Guo, Z. Y. Gu, X. T. Wang, X. X. Zhao, W. H. Li, H. Y. Yu, X. L. Wu, *Nano Res.* **2022**, *15*, 925-932; b) P. Jaumaux, J. R. Wu, D. Shanmukaraj, Y. Z. Wang, D. Zhou, B. Sun, F. Y. Kang, B. H. Li, M. Armand, G. X. Wang, *Adv. Funct. Mater.* **2021**, *31*, 2008644.

[10] J. Pan, N. N. Wang, H. J. Fan, *Small Methods* **2022**, *6*, 2201032.

[11] a) Y. Lu, L. Li, Q. Zhang, Z. Q. Niu, J. Chen, *Joule* **2018**, *2*, 1747-1770; b) J. Pan, P. Zhao, N. N. Wang, F. Q. Huang, S. X. Dou, *Energy Environ. Sci.* **2022**, *15*, 2753-2775.

[12] R. Asakura, D. Reber, L. Duchene, S. Payandeh, A. Remhof, H. Hagemann, C. Battaglia, *Energy Environ. Sci.* **2020**, *13*, 50485058.

[13] W. R. Hou, X. W. Guo, X. Y. Shen, K. Amine, H. J. Yu, J. Lu, *Nano Energy* **2018**, *52*, 279-291.

[14] a) C. L. Zhao, L. L. Liu, Y. X. Lu, M. Wagemaker, L. Q. Chen, Y. S. Hu, *Angew. Chem. Int. Ed.* **2019**, *58*, 17026-17032; b) S. L. Chen, H. Y. Che, F. Feng, J. P. Liao, H. Wang, Y. M. Yin, Z. F. Ma, *ACS Appl. Mater. Interfaces* **2019**, *11*, 43056-43065; c) H. C. Gao, L. G. Xue, S. Xin, K, Park, J. B. Goodenough, *Angew. Chem. Int. Ed.* **2017**, *56*, 5541-5545.

[15] a) X. E. Wang, C. Zhang, M. Sawczyk, J. Sun, Q. H. Yuan, F. F. Chen, T. C. Mendes, P. C. Howlett, C. K. Fu, Y. Q. Wang, X. Tan, D. J. Searles, P. Kral, C. J. Hawker, A. K. Whittaker, M. Forsyth, *Nature Mater.* **2022**, *21*, 1057-1065; b) S. L. Chen, F. Feng, H. Y. Che, Y. M. Yin, Z. F. Ma, *Chem. Eng. J.* **2021**, *406*, 126736; c) J. Pan, Y. C. Zhang, J. Wang, Z. C. Bai, R. G. Cao, N. N. Wang, S. X. Dou, F. Q. Huang, *Adv. Mater.* **2022**, *34*, 2107183; d) J. K. Kim, Y. J. Lim, H. Kim, G. B. Cho, Y. Kim, *Energy Environ. Sci.* **2015**, *8*, 3589-3596.

[16] a) Z. P. Li, P. Liu, K. J. Zhu, Z. Y. Zhang, Y. C. Si, Y. J. Wang, L. F. Jiao, *Energy Fuels* **2021**, *35*, 9063-9079; b) J. Pan, H. L. Peng, Y. H. Yan, Y. Z. Bai, J. Yang, N. N. Wang, S. X. Dou, F.Q. Huang, *Energy Storage Mater.* **2021**, *43*, 165-171; c) J. J. Zhang, J. H. Zhao, L. P. Yue, Q. F. Wang, J. C. Chai, Z. H. Liu, X. H. Zhou, H. Li, Y. G. Guo, G. L. Cui, L. Q. Chen, *Adv. Energy Mater.* **2015**, *5*, 1501082.

[17] a) S. Jahangiri, N. J. Mosey, *J. Phys. Chem. C* **2018**, *122*, 25785-25795; b) Q. Zhou, J. Ma, S. M. Dong, X. F. Li, G. L. Cui, *Adv. Mater.* **2019**, *31*, 1902029; c) Z. A. Yu, H. S. Wang, X. Kong, W. Huang, Y. Tsao, D. G. Mackanic, K. C. Wang, X. C. Wang, W. X. Huang, S. Choudhury, Y. Zheng, C. V. Amanchukwu, S. T. Hung, Y. T. Ma, E. G. Lomeli, J. Qian, Y. Cui, Z. N. Bao, *Nat. Energy* **2020**, *5*, 526-533; d) F. Wu, K. Zhang, Y. R. Liu, H. C. Gao, Y. Bai, X. R. Wang, C. Wu, *Energy Storage Mater.* **2021**, *33*, 26-54.

[18] a) D. H. Kim, B. Kang, H. Lee, *J. Power Sources* **2019**, *423*, 137-143; b) X. N. Chen, X. H. Wang, D. Fang, *Fuller. Nanotub. Carbon Nanostructures* **2020**, *28*, 1048-1058.; c) J. Q. Huang, X. Y. Guo, X. Q. Du, X. Y. Lin, J. Q. Huang, H. Tan, Y. Zhu, B. Zhang, *Energy Environ. Sci.* **2019**, *12*, 1550-1557; d) H. P. Wang, C. L. Zhu, J. D. Liu, S. H. Qi,

This article is protected by copyright. All rights reserved.

15213773, ja, Downloaded from https://onlinelibrary.wiley.com/doi/10.1002/anie.202219000 by NANYANG TECHNOLOGICAL UNIVERSITY, Wiley Online Library on [04/03/2023]. See the Terms and Conditions (https://onlinelibrary.wiley.com/terms-and-conditions) on Wiley Online Library for rules of use; OA articles are governed by the applicable Creative Commons License

Accepted Manuscript

M. G. Wu, J. D. Huang, D. X. Wu, J. M. Ma, *Angew. Chem.Int. Ed.* **2022**, *61*, e202208506.

[19] a) L. Zielke, F. Sun, H. Markotter, A. Hilger, R. Moroni, R. Zengerle, S. Thiele, J. Banhart, I. Manke, *ChemElectroChem* **2016**, *3*, 1170-1177; b) F. Sun, D. Zhou, X. He, M. Osenberg, K. Dong, L. B. Chen, S. L. Mei, A. Hilger, H. Makotter, Y. Lu, S. M. Dong, S. Marathe, C. Rau, X. Hou, J. Li, M. C. Stan, M. Winter, R. Dominko, I. Manke, *ACS Energy Lett.* **2020**, *5*, 152-161; c) F. Sun, L. Duchene, M. Osenberg, S. Risse, C. Yang, L. B. Chenm, N. Chen, Y. X. Huang, A. Hilger, K. Dong, T. Arlt, C. Battaglia, A. Remhof, I. Manke, R. J. Chen, *Nano Energy* **2021**, *82*, 105762; d) F. Sun, M. Osenberg, K. Dong, D. Zhou, A. Hilger, C. J. Jafta, S. Risse, Y. Lu, H. Markotter, I. Manke, *ACS Energy Lett.* **2018**, *3*, 356-365.

[20] a) X. Wang, X. P. Yin, X. C. Feng, Y. Li. X. P. Dong, Q. H. Shi, Y. F. Zhao, J. J. Zhang, *Chem. Eng. J.* **2022**, *428*, 130990; b) E. Matios, H. Wang, J. M. Luo, Y. W. Zhang, C. L. Wang, X. Lu, X. F. Hu, Y. Xu, W. Y. Li, *J. Mater. Chem. A* **2021**, *9*, 18632-18643; c) B. W. Xiao, Y. C. Wang, S. Tan, M. Song, X. Li, Y. X. Zhang, F. Lin, K. S. Han, F. Omenya, K. Amine, X. Q. Yang, D. Reed, Y. Y. Hu, G. L. Xu, E. Y. Hu, X. Li, X. L. Li, *Angew. Chem. Int. Ed.* **2021**, *60*, 8258-8267.

WILEY-VCH

This article is protected by copyright. All rights reserved.

15213773, ja, Downloaded from https://onlinelibrary.wiley.com/doi/10.1002/anie.202219000 by NANYANG TECHNOLOGICAL UNIVERSITY, Wiley Online Library on [04/03/2023]. See the Terms and Conditions (https://onlinelibrary.wiley.com/terms-and-conditions) on Wiley Online Library for rules of use; OA articles are governed by the applicable Creative Commons License

10.1002/anie.202219000

WILEY-VCH

COMMUNICATION

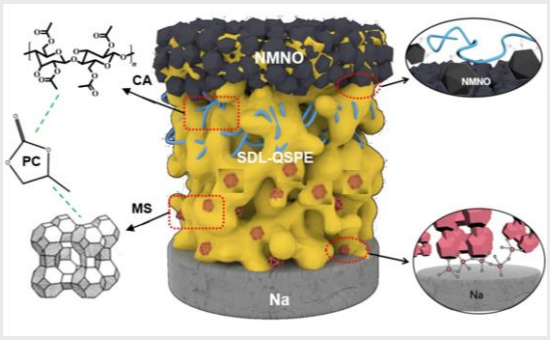

*Jun Pan[#], Yuchen Zhang[#], Fu Sun, Markus Osenberg, André Hilger, Ingo Manke, Ruiguo Cao, Shi Xue Dou, Hong Jin Fan**

Page No. – Page No.

Designing Solvated Double-Layer Polymer Electrolytes with Molecular Interactions Mediated Stable Interfaces for Sodium Ion Batteries

A solvated double-layer quasi-solid polymer electrolyte is rationally designed for two purposes: enhance the interfacial stability and Na ion conductance. The double-layer structure is laminated by cathode- and anode-facing polymer electrolytes to meet the different interfacial requirements. Meanwhile, different functional fillers are solvated with plasticizer to improve the Na^+ conductivity and thermal stability.

This article is protected by copyright. All rights reserved.

15213773, ja, Downloaded from https://onlinelibrary.wiley.com/doi/10.1002/anie.202219000 by NANYANG TECHNOLOGICAL UNIVERSITY, Wiley Online Library on [04/03/2023]. See the Terms and Conditions (https://onlinelibrary.wiley.com/terms-and-conditions) on Wiley Online Library for rules of use; OA articles are governed by the applicable Creative Commons License

WILEY-VCH Accepted Manuscript